Supporting information:

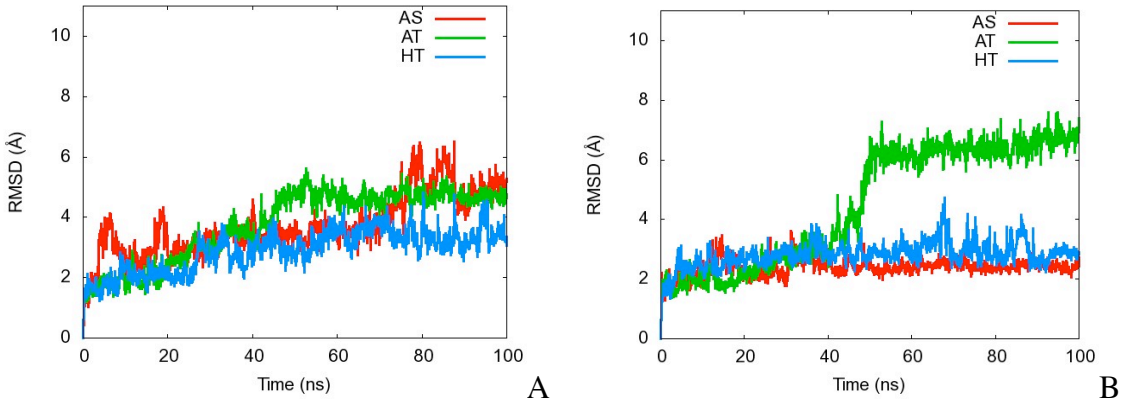


**Figure SI-1A,B**. $C_\alpha$ RMSD of the DBDs for the AB and CD wings respectively. For both AS and HT the DBD RMSD stays relatively low on the CD side but gradually rises on the AB side. The AB wing of the AT simulation also rises gradually, but the CD side changes dramatically between the 45$^{th}$ and 55$^{th}$ ns.

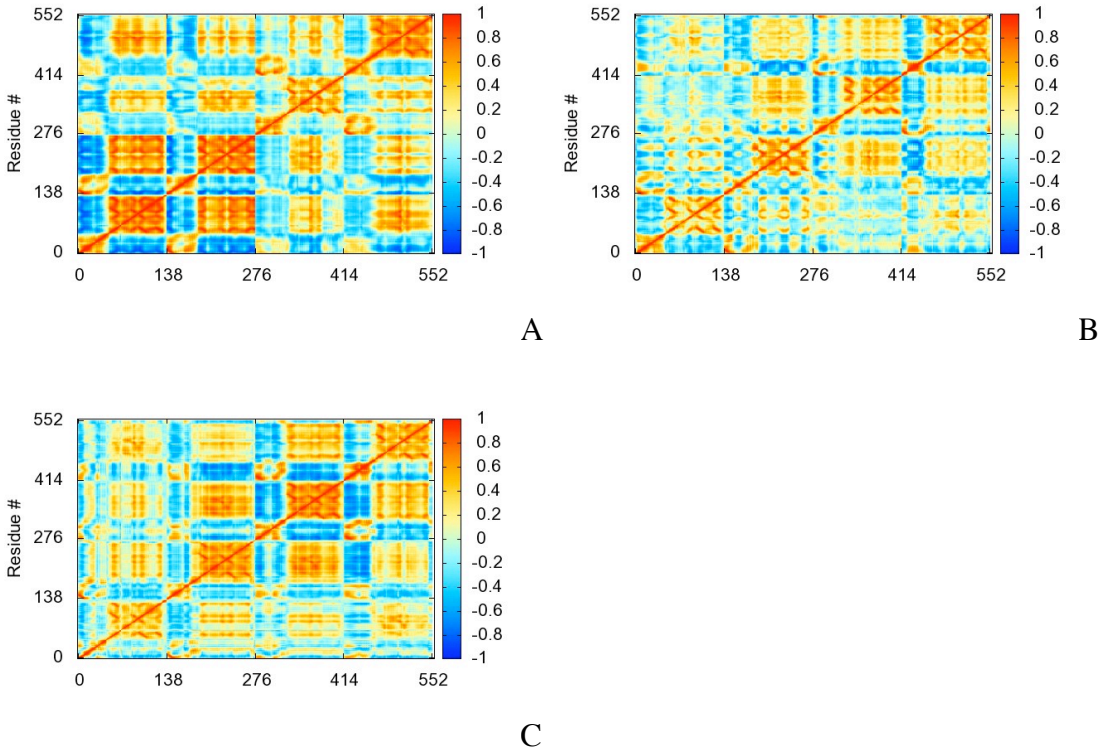


**Figure SI-2A-C**. Correlation matrices for all three simulations. A, B, and C are the AS, AT, and HT simulations, respectively.

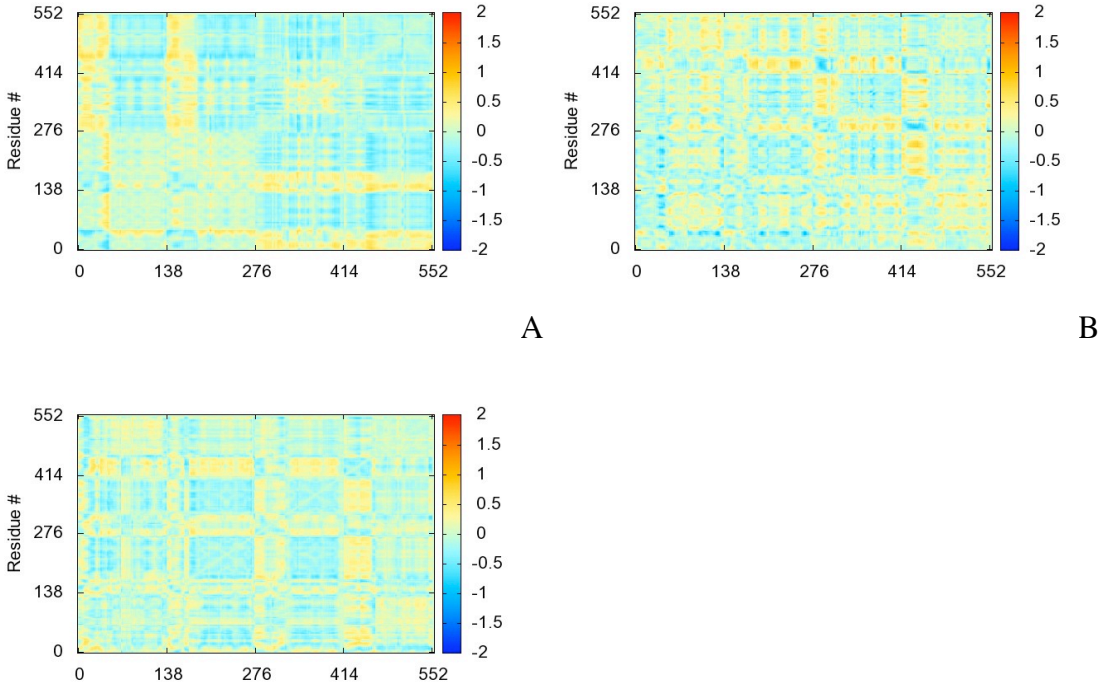


**Figure SI-3A-C**. Correlation change between first and second halves of each simulation. A, B and C show correlation difference for AS, AT, and HT simulations respectively. The correlation of the $10^{th}$-$45^{th}$ ns was subtracted from the $45^{th}$ to $80^{th}$ ns of the same simulation (each correlation matrix element was subtracted from its equivalent counterpart. These correlation differences are shown in Figures 15A-C on a scale (-2:2) double the original (-1:1). A value of +2 indicates that the interaction went from being anti-correlated to correlated. The graphs indicate no significant change in correlation between the first and second halves of the simulation. For the AS, AT, and HT simulations there were 2, 14, and 0 changes in correlation greater in magnitude than 1.

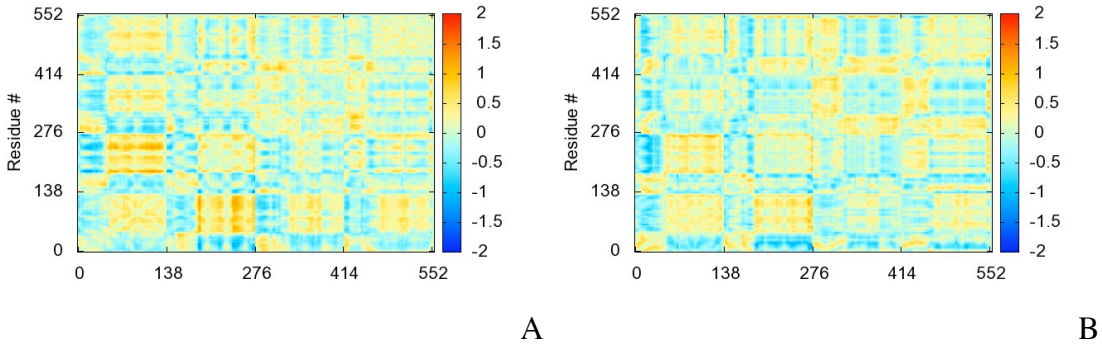

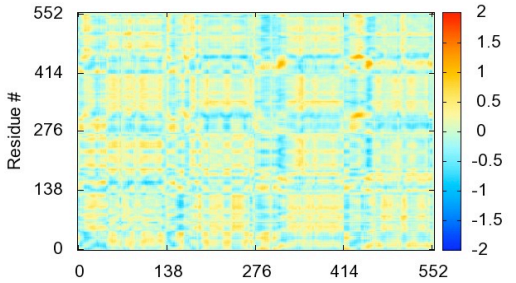


C

**Figures SI-4A-C**. Correlation difference between simulations. Figures SI-4A-C show the correlation differences, $C_{ij}^{AS} - C_{ij}^{AT}$ ,$C_{ij}^{AS} - C_{ij}^{HT}$ , and $C_{ij}^{HT} - C_{ij}^{AT}$ respectively. For each comparison, the magnitude of the correlation difference was greater than 1 a total of 128, 150, and 31 times for the $C_{ij}^{AS} - C_{ij}^{AT}$ ,$C_{ij}^{AS} - C_{ij}^{HT}$ , and $C_{ij}^{HT} - C_{ij}^{AT}$ respectively. Interestingly this suggests that despite the difference in behavior between HT and AT (which began from the same structure) based on RMSD analysis, the inter-residue correlations are very similar.

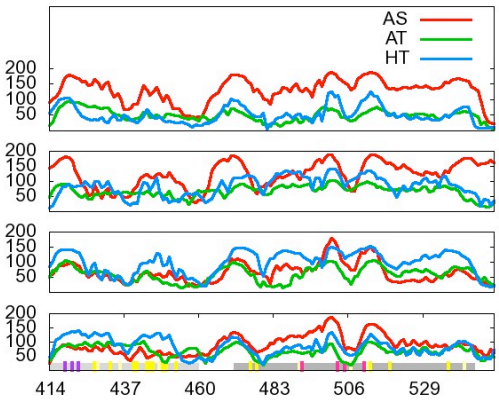


**Figure SI-5**. Correlation difference between simulations not summed over chain

Correlation relevance can also be filtered into those only crossing domains:

$$xDREL_i = \sum_{j=1}^{N} \left| c_{i,j} \right| \cdot \frac{\xi(i,j)}{n(D(j))} \qquad \text{(Equation SI-1)}$$

$$\xi(i,j) = \begin{cases} 0 & D_i = D_j \\ 1 & otherwise \end{cases} \qquad \text{(Equation SI-2)}$$

Here, $D_i$ is the domain of residue *i* (DBD or MBD) and $n(D(j))$ is the number of residues in domain type D. These values were plotted either by residue or summed over chains in Figures SI-6A,B with linking residues removed. Similar to the previous chain-independent graph, the AS and HT have nearly identical behavior in the DBD. The MBD regions act more similarly between AS and HT forms. This could indicate that although the MBD of AS form is much more coupled than HT form, the cross-domain interactions

are similar. It appears as though both the nickel-binding and DNA-binding residues have strong interdomain interactions. This is could be a result of the allosteric mechanism.

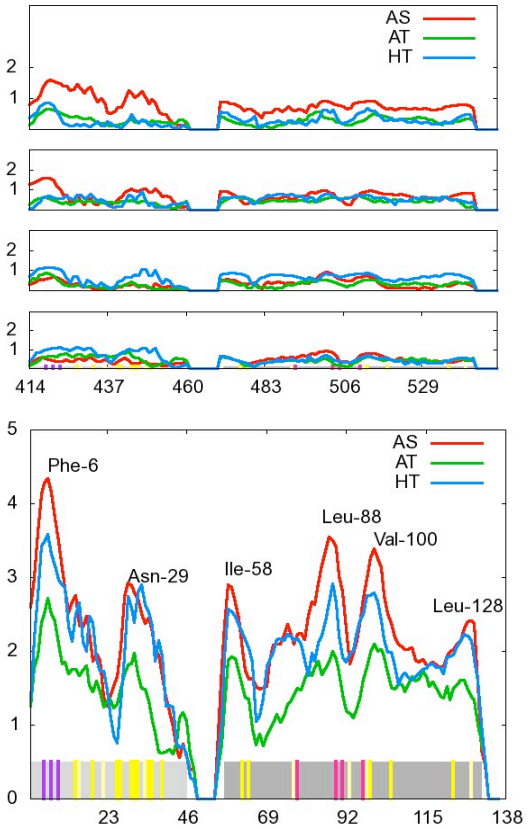


**Figures SI-6A,B**. Cross-correlation relevance graphs for each simulation. A) Cross-correlation relevance by residue (x$DREL_i$). B) Cross-correlation relevance summed over chains (cx$DREL_i$)

It is likely that in this allosteric system, the "biologically important" residues indicated by the colored bars at the bottom of Figures SI-6A,B and SI-6A,B will have a strong impact on cross-domain correlation. Table SI-1 shows the averaged cross-domain correlation relevance for each form for different sets of biologically important residues. As the criterion for biological importance becomes stricter, the average cross-domain correlation increases.

| | All | B,F,M | B,F | B |
|---|---|---|---|---|
| AS | 2.22 | 2.59 | 2.65 | 3.32 |
| AT | 1.44 | 1.62 | 1.67 | 2.00 |
| HT | 1.97 | 2.35 | 2.38 | 2.83 |

**Table SI-1:** Average cross-domain relevance for various forms of NikR. The column marked all considers all residues for which the cross-domain relevance was considered. B is for either nickel or DNA binding residues, F is for fully conserved residues, and M is for mostly conserved residues.

Figures SI-7A-D show RMSD against initial structure of the C terminal domains of each chain. X-ray data show that each symmetry-related half contains one free loop (A

and D chains) and one ion-stabilized loop (B and C). Interestingly, in the AS form, the loop is stabilized by a negative chloride ion, and in the holo – trans form, it is stabilized by a positively charged nickel ion. For the simulations, neither ion was included in the model. The only loop that fluctuates more than 2Å is the A-loop for the AS, and AT simulations. There seems to be very little correlation between either the different loops of the same simulation or the same loop for different simulations. This suggests that the loop motion is independent of conformation and the presence of the four primary nickel ions.

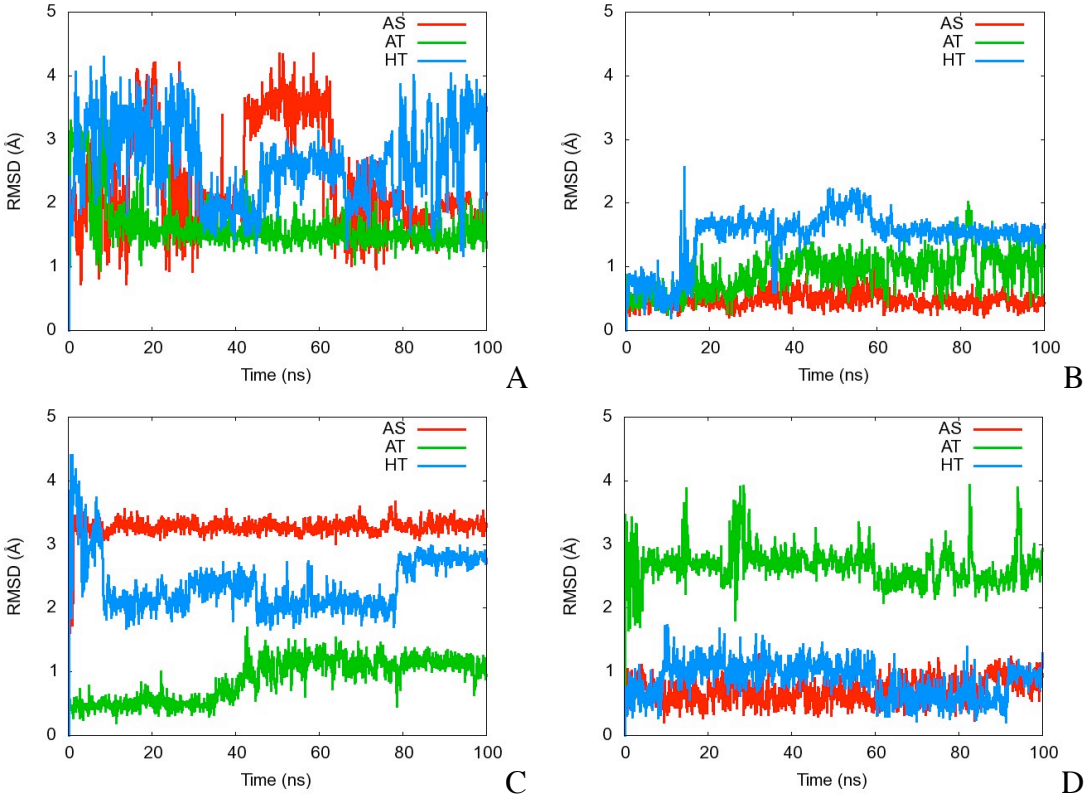


**Figure SI-7 A-D.** $C_\alpha$ RMSD for the C-terminal loops for all simulations. Figures A-D are for chains A,B,C and D respectively.

*MBD DNA contact loop*

Schreiter *et al*. also found loops in the MBD that make noncovalent contacts with DNA[18]. The RMSD of these loops (residues 64-67) are shown in Figures SI-8A-D. Similar to the C-terminal loop, in the absence of DNA and ions other than the primary nickel ions, no correlation can be seen between the three forms in this region of the protein.

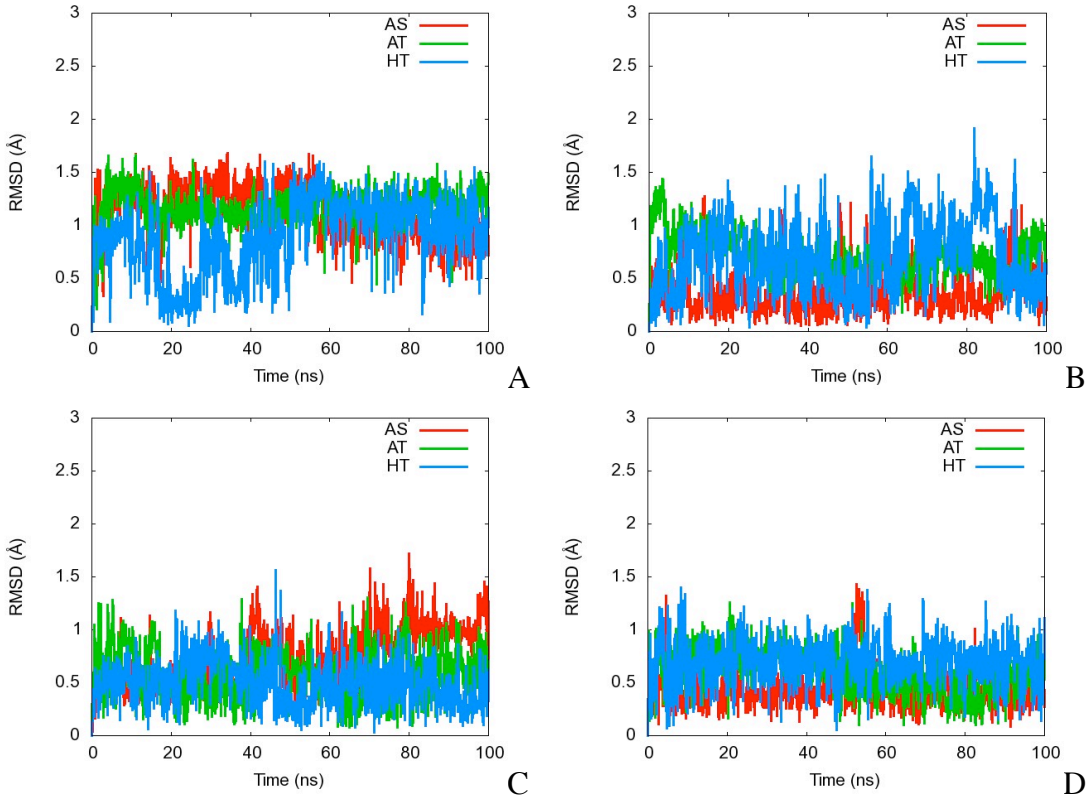


**Figures SI-8A-D**. $C_\alpha$ RMSD for "DNA touching loop", residues 64-67 of each chain. Figures A-D show chains A,B,C and D respectively.

*RMS fluctuations:*

To observe the stability of the protein, RMS fluctuations of the $C_\alpha$ atom of each residue of the protein were measured for each form. Figures SI-9A-D show the fluctuations by residue of each chain (A,B,C,D). The figures indicate, not unexpectedly, that the DBDs (wings) fluctuate much more wildly than the MBDS. As seen in the RMSD plots, the two experimentally observed forms (AS and HT) behave similarly, especially in the MBD. The AT form seems much less stable, especially in the MBD. The AB wing (DBD) of the AS form seems to fluctuate much more wildly than its dimeric counterpart (the CD wing).

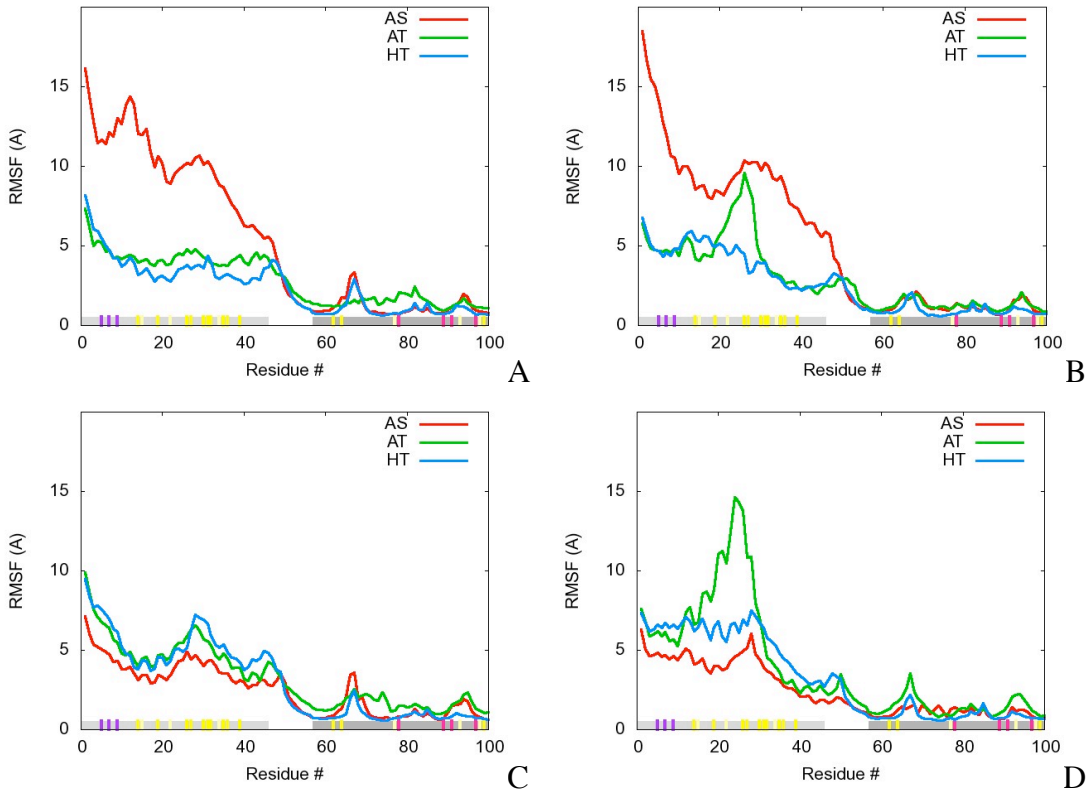


**Figure SI-9A-D.** RMS fluctuations of the $C_\alpha$ atom for each chain of each simulation. Figures A-D represent chains A, B, C, and D respectively.

## Force field parameters

Partial charges:

| C97A | H87A | H89A | H78D |
|---|---|---|---|

| Amber Atom ID/Type | Charge | AMBER Atom ID/Type | Charge | AMBER Atom ID | Charge | AMBER Atom ID | Charge |
|---|---|---|---|---|---|---|---|
| N/N | -0.463 | N/N | -0.4157 | N/N | -0.4157 | N/N | -0.4157 |
| HN/H | 0.252 | H/H | 0.2719 | H/H | 0.2719 | H/H | 0.2719 |
| CA/CT | 0.035 | CA/CT | 0.0188 | CA/CT | -0.0581 | CA/CT | 0.0188 |
| HA/H1 | 0.048 | HA/H1 | 0.0881 | HA/H1 | 0.136 | HA/H1 | 0.0881 |
| CB/CT | 0.21679 | CB/CT | -0.32182 | CB/CT | 0.0838 | CB/CT | -0.04799 |
| HB3/H1 | 0.01975 | HB2/H1 | 0.18394 | HB2/HC | 0.06662 | HB2/HC | 0.07776 |
| HB2/H1 | 0.01975 | HB3/H1 | 0.18394 | HB3/HC | 0.06662 | HB3/HC | 0.07776 |
| SG/**S1** | -0.52432 | CG/CC | -0.1281 | CG/CC | 0.04537 | CG/CC | 0.10735 |
| C/C | 0.616 | ND1/NA | -0.04524 | ND1/**NY** | 0.0069 | ND1/NA | -0.3257 |
| O/O | -0.504 | HD1/H | 0.29485 | CE1/CR | -0.1906 | HD1/NA | 0.37104 |
| | | CE1/CR | 0.04268 | HE1/H5 | 0.20125 | CE1/CR | 0.04183 |

| | | | | | | | |
|---|---|---|---|---|---|---|---|
| | | HE1/H5 | 0.14435 | NE2/NA | -0.08532 | HE1/H5 | 0.20837 |
| | | NE2/**NZ** | -0.66101 | HE2/H | 0.31809 | NE2/**NX** | -0.16857 |
| | | CD2/CV | 0.21993 | CD2/CW | -0.22892 | CD2/CV | -0.24011 |
| | | HD2/H4 | 0.03232 | HD2/H4 | 0.19764 | HD2/H4 | 0.14371 |
| | | C/C | 0.5973 | C/C | 0.5973 | C/C | 0.5973 |
| | | O/O | -0.5679 | OO | -0.5679 | O/O | -0.5679 |

Bond stretching

| Bonds | Force Constant (Kcal/mol/A^2) | Distance (A) |
|---|---|---|
| CT-S1 | 237 | 1.81 |
| HS-S1 | 274 | 1.336 |
| LP-S1 | 600 | 0.7 |
| CB-NZ | 414 | 1.391 |
| CK-NZ | 529 | 1.304 |
| CC-NZ | 410 | 1.394 |
| CR-NZ | 488 | 1.335 |
| CV-NZ | 410 | 1.394 |
| LP-NZ | 600 | 0.2 |
| CB-NY | 414 | 1.391 |
| CK-NY | 529 | 1.304 |
| CC-NY | 410 | 1.394 |
| CR-NY | 488 | 1.335 |
| CV-NY | 410 | 1.394 |
| LP-NY | 600 | 0.2 |
| CB-NX | 414 | 1.391 |
| CK-NX | 529 | 1.304 |
| CC-NX | 410 | 1.394 |
| CR-NX | 488 | 1.335 |
| CV-NX | 410 | 1.394 |
| LP-NX | 600 | 0.2 |
| NI-NZ | 97.34 | 2.038 |
| NI-NY | 66.24 | 2.062 |
| NI-S1 | 92.81 | 2.206 |
| NI-NX | 89.89 | 2.017 |

Angle bending

| ANGL | Kcal/mol/rad^2 | Angle (degrees) |
|---|---|---|
| H1-CT-S1 | 50 | 109.5 |
| CT-CT-S1 | 50 | 108.6 |
| CT-S1-HS | 43 | 96 |
| HS-S1-HS | 35 | 92.07 |
| CT-S1-LP | 50 | 90 |
| LP-S1-LP | 50 | 180 |

| | | |
|---|---|---|
| HS-S1-LP | 50 | 90 |
| C-CB-NZ | 70 | 130 |
| CA-CB-NZ | 70 | 132.4 |
| CB-CB-NZ | 70 | 110.4 |
| H5-CK-NZ | 50 | 123.05 |
| N*-CK-NZ | 70 | 113.9 |
| CT-CC-NZ | 70 | 120 |
| CW-CC-NZ | 70 | 120 |
| H5-CR-NZ | 50 | 120 |
| NA-CR-NZ | 70 | 120 |
| CC-CV-NZ | 70 | 120 |
| H4-CV-NZ | 50 | 120 |
| CB-NZ-CK | 70 | 103.8 |
| CC-NZ-CR | 70 | 117 |
| CR-NZ-CV | 70 | 117 |
| CB-NZ-LP | 50 | 126 |
| CC-NZ-LP | 50 | 126 |
| CK-NZ-LP | 50 | 126 |
| CR-NZ-LP | 50 | 126 |
| CV-NZ-LP | 50 | 126 |
| C-CB-NY | 70 | 130 |
| CA-CB-NY | 70 | 132.4 |
| CB-CB-NY | 70 | 110.4 |
| H5-CK-NY | 50 | 123.05 |
| N*-CK-NY | 70 | 113.9 |
| CT-CC-NY | 70 | 120 |
| CW-CC-NY | 70 | 120 |
| H5-CR-NY | 50 | 120 |
| NA-CR-NY | 70 | 120 |
| CC-CV-NY | 70 | 120 |
| H4-CV-NY | 50 | 120 |
| CB-NY-CK | 70 | 103.8 |
| CC-NY-CR | 70 | 117 |
| CR-NY-CV | 70 | 117 |
| CB-NY-LP | 50 | 126 |
| CC-NY-LP | 50 | 126 |
| CK-NY-LP | 50 | 126 |
| CR-NY-LP | 50 | 126 |
| CV-NY-LP | 50 | 126 |
| C-CB-NX | 70 | 130 |
| CA-CB-NX | 70 | 132.4 |
| CB-CB-NX | 70 | 110.4 |
| H5-CK-NX | 50 | 123.05 |
| N*-CK-NX | 70 | 113.9 |
| CT-CC-NX | 70 | 120 |
| CW-CC-NX | 70 | 120 |
| H5-CR-NX | 50 | 120 |

| | | |
|---|---|---|
| NA-CR-NX | 70 | 120 |
| CC-CV-NX | 70 | 120 |
| H4-CV-NX | 50 | 120 |
| CB-NX-CK | 70 | 103.8 |
| CC-NX-CR | 70 | 117 |
| CR-NX-CV | 70 | 117 |
| CB-NX-LP | 50 | 126 |
| CC-NX-LP | 50 | 126 |
| CK-NX-LP | 50 | 126 |
| CR-NX-LP | 50 | 126 |
| CV-NX-LP | 50 | 126 |
| CV-NX-NI | 119.045 | 120.926 |
| S1-NI-NX | 135.003 | 85.768 |
| NZ-NI-NY | 98.051 | 88.68 |
| NZ-NI-S1 | 125.6 | 95.101 |
| NZ-NI-NX | 86.915 | 176.994 |
| CR-NX-NI | 114.211 | 126.433 |
| CR-NY-NI | 100.446 | 115.058 |
| CC-NY-NI | 109.757 | 135.465 |
| CV-NZ-NI | 110.423 | 131.46 |
| CT-S1-NI | 128.037 | 107.681 |
| NY-NI-S1 | 96.174 | 173.922 |
| NY-NI-NX | 103.035 | 90.697 |
| CR-NZ-NI | 110.488 | 118.865 |